Energy 41 (2012) 514–524

Contents lists available at SciVerse ScienceDirect

Energy

journal homepage: www.elsevier.com/locate/energy

Design and experimental study of ORC (organic Rankine cycle) and radial turbine using R245fa working fluid

Seok Hun Kang*

Korea Atomic Energy Research Institute, Daedeok-daero 989-111, Yuseong-gu, Daejeon 305-353, South Korea

ARTICLE INFO

Article history:
Received 10 November 2011
Received in revised form
16 January 2012
Accepted 16 February 2012
Available online 22 March 2012

Keywords:
ORC (Organic Rankine cycle)
R245fa
Turbine
Power generation

ABSTRACT

In this study, an ORC (Organic Rankine Cycle) capable of generating electric power using a low-temperature heat source was developed and an experimental study was conducted. A radial turbine directly connected to the high-speed synchronous generator was also designed and developed. R245fa was adopted as a working fluid, in consideration of the operation conditions of the cycle and its environmentally-friendly characteristics. Experiments were conducted to analyze the operational characteristics and performance of the developed ORC. The efficiencies of the cycle and the turbine, electric power of the developed ORC with respect to the operation conditions were investigated in a series of experiments. The factors which influence the performance of the developed ORC were analyzed and discussed.

1. Introduction

Recently, oil prices have been fluctuating dramatically due to the expansion of various economies around the world, particularly those of China and India, to conflicts in the Middle East, and to the enforcement of stricter environmental regulations concerning greenhouse gas emissions. Under these circumstances, research on the ORC (organic Rankine cycle), which could convert low-grade heat to electric power, has been attracting more attention as a high efficiency energy technology in recent decades [1]. The ORC is understood as the most realized one among several proposed technologies for generating electricity via the utilization of low-grade heat sources. Therefore, it is capable of enhancing energy utilization and reducing greenhouse gas emissions [2]. In addition to this, the ORC offers a number of advantages such as its simple structure, the availability of its components, and the easiness of its application to local small-scale power generation systems.

The ORC is structurally similar to a typical Rankine cycle but uses organic fluids as a working fluid instead of water. Organic fluids are suitable for the ORC because their specific vaporization heat is much lower than that of water. This enables the ORC to produce electricity by using low-temperature heat sources. The ORC is mainly used as a power generation system utilizing low-grade heat sources, and has a temperature range of 60–200 °C [3–6]. Generally, heat is considered to be moderate-to-low grade when it is less than 370 °C [2]. In the energy-to-power conversion industry, thermal efficiency becomes uneconomically low when the exhaust-stream temperature drops below 370 °C. However, recovering low-grade waste heat in power generation becomes economically viable when using ORCs. It has been estimated statistically that low-grade waste heat accounts for more than 50% of the total amount of heat generated in industry [7].

The ORC is not merely the subject of laboratory studies as more than one hundred ORC plants are now operating to generate electricity commercially, and the ORC has also applied to diverse fields including industrial waste heat, solar thermal power, geothermal heat, biomass combustion heat, engine exhaust gases and so forth [1]. ORC manufacturers such as ORMAT, Turboden, BNI, Adoratec, UTC, and Electratherm have been present on the market since the beginning of the 1980s. All of them use the turbine as an expander, except Electratherm, which uses a screw expander [8]. Large-scale ORC plants have been successfully demonstrated, such as in the geothermal plant in Altheim, and in the biomass-fired CHP plants in Admont, Lienz and Heidelberg [9]. In Europe more than 120 ORC plants are in commercial operation, with sizes ranging from 0.2 to 2.5 MW, using biomass combustion heat [10].

The expander is a key part of the ORC system, and two types of expander, the turbo and the scroll, are generally used [8]. The scroll expander is a good candidate for the expansion device of small-scale ORC systems because of its simple operation, low rotational

* Tel.: +82 42 868 8080; fax: +82 42 868 2075.
E-mail addresses: shkang73@gmail.com, kang@kaeri.re.kr.

0360-5442/$ – see front matter © 2012 Elsevier Ltd. All rights reserved.
doi:10.1016/j.energy.2012.02.035

speed, reliability, and capability to handle high-pressure ratio [1]. The turbo expander, on the other hand, offers many advantages, such as its compact structure, small size, light weight, stability, superior and efficiency, and the majority of commercial ORC plants use it [8,9].

Nguyen et al. developed and tested a small-scale ORC which used *n*-pentane as a working fluid and was driven by heat sourced from a gas-fired boiler. The developed system was capable of generating 1.5 kW of electricity with a thermal efficiency of 4.3% [11]. Manolakos et al. presented their on-site experimental evaluation of the performance of a low-temperature ORC for reverse osmosis desalination. The system used R134a as the working fluid and obtained technically feasible results [12]. Quoiin et al. performed a numerical and experimental study on an ORC which used R123 as the working fluid and a scroll expander. The scroll expander was originally an oil-free open-drive scroll compressor, adapted to operate in reverse. It was used to drive an asynchronous machine through two belt-pulley couplings and a torque meter used to measure the expander shaft power [1]. Wang et al. developed a concept that combines an ORC with a conventional vapor compression cycle. They developed a 5 kW cooling capacity prototype system which used R245fa (1,1,1,3,3-pentafluoropropane) as the working fluid and tested it under laboratory conditions. The system used micro-channel-based heat transfer components and a scroll-based expander and compressor. The scroll expander is a positive displacement scroll compressor modified to operate in reverse [2]. Larjola designed an ORC using a high-speed oil-free turbo generator-feed pump [13]. Yamamoto et al. designed an ORC by using an electric evaporator instead of an external heat source. R123 and water were used as the working fluids and experiments were conducted to compare each fluid. Its maximum cycle efficiency and electric power were shown to be 1.25% and 150 W, respectively [3]. Pei et al. constructed an ORC system with a turbine using R123 and conducted a preliminary test on the constructed system. The cycle efficiency, based on electric power and turbine shaft power, was shown to be 3.0% and 1 kW, respectively. In addition, several problem-solving techniques were presented, such as the avoidance of cavitation in the pump [9].

Previous studies also showed the influence of the working fluid thermodynamic properties on ORC performance [14–19,32]. Hung et al. parametrically analyzed the effects of various working fluids such as benzene, ammonia, R11, R12, and R134a on the efficiency of ORCs. They showed that the slopes and shapes of the saturated vapor curves of the fluids primarily affected system efficiency [20,21]. Hettiarachchi et al. presented a cost-effective optimum design criterion for ORCs utilizing low-temperature geothermal heat sources. The optimum cycle performance was compared for various working fluids including ammonia, HCFC123, *n*-Pentane, and PF5050 [22]. Wei et al. conducted a system performance analysis and optimization of an ORC system using R245fa as the working fluid and driven by exhaust heat. They also analyzed the thermodynamic performances of an ORC system when subjected to disturbances [6]. Aljundi analyzed the effects of using alternative dry fluids on the efficiency of the ORC and compared them with other refrigerants [23]. Rayegan et al. developed a procedure for comparing the capabilities of working fluids when they are employed in a solar ORC under similar working conditions. They considered the REFPROP 8.0 [24] database with 117 organic fluids as the reference [25]. Suna et al. developed mathematical models and an optimization approach to simulate an ORC power plant, and searched for optimal operating strategies in order to achieve either the best thermal efficiency or the most net power generation [26] of the system.

Table 1
Properties of R245fa (HFC-245fa).

Molecular name	Molecular weight	Critical pressure	Critical temperature
$CF_3CH_2CHF_2$	134 g/mol	3640 kPa	427.2 K

Although many studies on ORCs have been conducted, only a few papers have presented an experimental study of an ORC equipped with an expander which could generate electricity. And most of the expanders thus employed were not designed considering cycle condition but obtained by modifying existing compressors, they showed low efficiencies lower than about 20% [1,2,9]. Therefore, the previous results showed low system performances that their cycle efficiency and electric power were lower than about 3% and 1.5 kW, respectively [3,9,11].

For the purposes of the present study, an ORC generating a nominal 30 kW of electric power was designed and an experimental study conducted. A radial turbine was also designed by considering the cycle operation condition and the thermodynamic properties of the working fluid (R245fa) to increase its performance. A high-speed synchronous generator was directly coupled

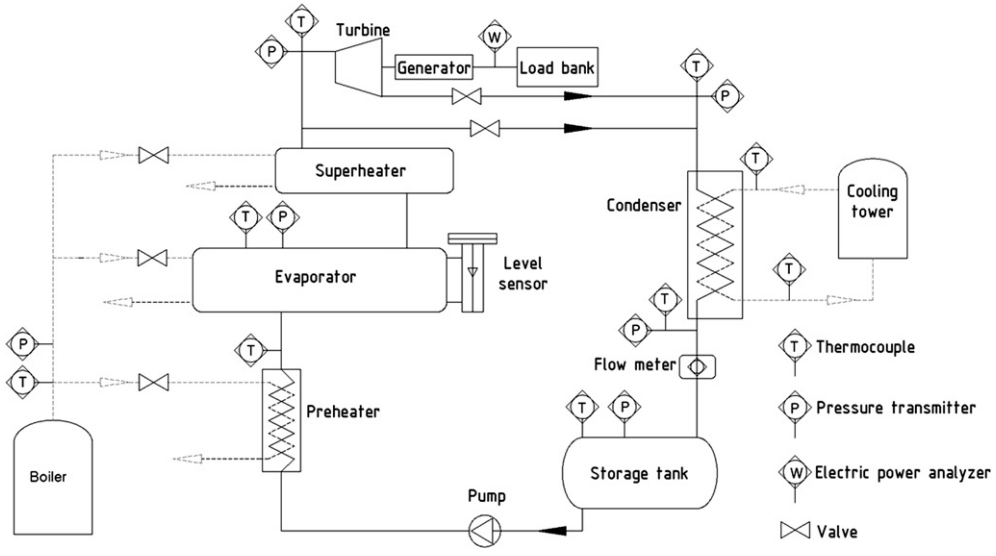

Fig. 1. Schematic diagram of the designed ORC system.

with a turbine blade to generate electricity without reducing speed and efficiency. R245fa was selected as a working fluid on the basis of the following characteristics: It is suitable for cycle operation conditions because it provides the appropriate evaporation pressure, creates overpressure on the condenser, and delivers good process efficiency. Furthermore, it is not subject to greenhouse gas emission regulations as it does not damage the ozone layer, and it is non-flammable, non-toxic, and has satisfactory thermal stability [2,13]. Table 1 shows the thermodynamic properties of R245fa [24]. The designed system showed increased performance in its efficiency and power output compared to the previous studies. This work represents a step forward in research on the design and experimental evaluation of an ORC under laboratory conditions.

2. Design of cycle and turbine

2.1. Cycle design

Fig. 1 is a schematic diagram of the designed ORC system. The steam and water circuits are represented by dashed lines, signifying the heat source and coolant, respectively. The thermodynamic cycle design process can be briefly described as follows. As the basis of the cycle design, condensation pressure was considered first and set to the saturation value, i.e., 1.78 bar, of the working fluid at 30 °C. The condensation temperature was determined to be 5–10 °C higher than atmospheric temperature in autumn. Generally, cycle efficiency increases as the pressure ratio between the turbine inlet and its outlet rises. However, the turbine was limited in terms of increasing the pressure ratio. A radial type of turbine whose pressure ratio between its inlet and outlet is 4.11 was designed (the design procedure is explained in the next section). Therefore, the evaporation pressure, which is considered to be the

Table 2
Thermodynamic properties of working fluid at cycle design points

Design points	T (°C)	P (bar)	h (kJ/kg)	s (kJ/kg-K)	Density (kg/m^3)
(a)	30	1.78	239	1.14	1325
(b)	77	7.32	305	1.34	1181
(c)	77	7.32	460	1.78	40.7
(d)	80	7.32	463	1.79	40.0
(e)	48	1.78	444	1.75	9.44
(f)	30	1.78	427	1.14	10.2

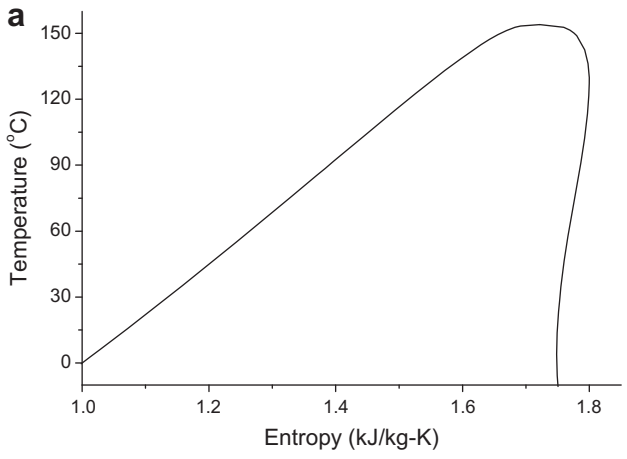

Positive slope of the saturated vapor curve of R245fa

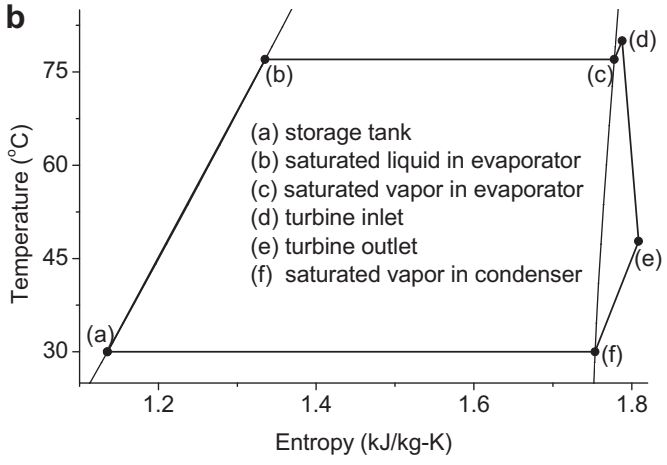

T-s diagram of the designed cycle

Fig. 2. *T–s* diagram. (a) Positive slope of the saturated vapor curve of R245fa; (b) *T–s* diagram of the designed cycle.

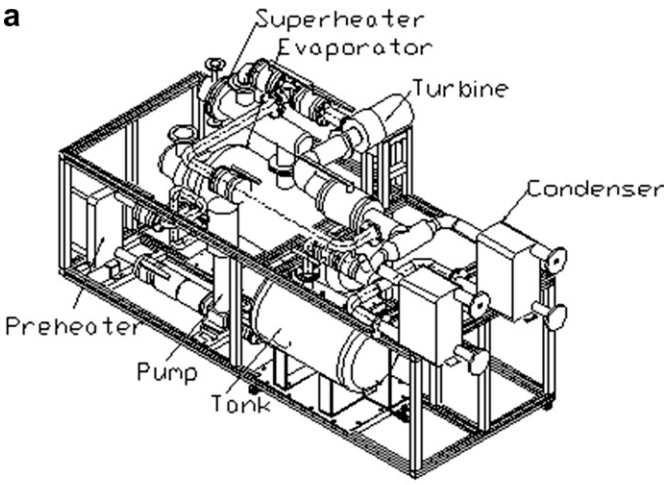

Schematic drawing

Photograph

Fig. 3. Schematic drawing and photograph of the developed ORC. (a) Schematic drawing; (b) Photograph.

Table 3
Physical properties of R245fa compared to air and steam at 5 atm, 200 °C.

	Unit	Air	Steam	R245fa
Speed of sound	m/s	436	527	177
Density	kg/m^3	3.7	2.4	17.6
Dynamic viscosity	μm^2/s	7.06	6.82	0.95

same as the turbine inlet pressure, was set to 7.32 bar in consideration of the condensation pressure and the pressure ratio at the turbine inlet and outlet, which is 4.11 (=7.32/1.78). The evaporation temperature was set to the saturation value, which is 77 °C, of the R245fa at the evaporation pressure. The ORC was designed to superheat the working fluid to 80 °C in order to increase its quality. The typical Rankine cycle, which uses water as its working fluid, requires a superheater to avoid any decrease in quality during the expansion process in the turbine. On the other hand, the present ORC, which uses R245fa, does not need a superheater, because saturated vapor curve in the temperature versus entropy (T–s) diagram for R245fa has a positive slope, as shown in Fig. 2(a), and liquid droplets are not formed during the expansion process, in contrast to water. Generally, a superheated approach for dry fluid such as R245fa is not appropriate and would even cause a decrease in ORC efficiency due to the limited temperature difference between the hot and cold sides [9,27,28]. Nevertheless, a superheater was used in this study to avoid the kind of decrease in quality that can be caused by heat loss. The working fluid mass flow rate was set to 1.58 kg/s to generate 30 kW theoretically, by designing the nozzle-throat area of the turbine under the above condition. Fig. 2(b) shows the T–s diagram of the designed cycle, and Table 2 lists the thermodynamic properties of the working fluid at the design points.

Cycle efficiency was calculated as 8.76% using Equation (1), ignoring pressure and heat loss in the entire system [29].

$$\eta_{th} = \frac{\dot{W}_t - \dot{W}_p}{\dot{m}\cdot(h_{s,o} - h_{p,o})} \quad (1)$$

where η_{th} is the cycle efficiency, $\dot{W}_t$ is the power output of the turbine measured by a power meter, $\dot{m}$ is the mass flow rate, $h_{s,o}$ is the specific enthalpy of the working fluid at the superheater outlet, $h_{p,o}$ is the specific enthalpy of the working fluid at the pump outlet, and $\dot{W}_p$ is the power consumed by the pump, which is calculated using Equation (2)

$$\dot{W}_p = \dot{m}\cdot(h_{p,o} - h_{p,i}) \quad (2)$$

where $h_{p,i}$ is the specific enthalpy of the working fluid at the pump inlet [9].

Fig. 3(a) and (b) shows a schematic drawing and a photograph of the developed experimental apparatus, respectively. The developed ORC consists of heat exchangers—i.e., a pre-heater, evaporator, superheater, and condenser—that heat or cool the working fluid, as well as a turbine, a pump and a storage tank.

Table 4
Preliminary design requirements of turbine.

Parameters	Unit	Values
Inlet temperature	°C	80
Inlet pressure	bar	7.32
Outlet pressure	bar	1.78
Mass flow rate	kg/s	1.58
Output power	kW	30
Rotational velocity	rpm	20,000
Efficiency	%	75

Table 5
Preliminary design results of turbine.

	Unit	Parameters	
		Nozzle	Blade
Outer diameter	mm	173	125
Number of blade		20	12
Inlet angle to radial direction	degree	0	0
Exit angle to radial direction	degree	75.9	57

A shell-and-tube type heat exchanger was used for the evaporator, since it must contain working fluid in both liquid and vapor states simultaneously to produce saturated vapor. The level of the liquid state working fluid in the evaporator was controlled by using a float-type level sensor and a circulation pump. The level sensor installed in the evaporator gives a signal to a control panel to control the pump, which maintains the liquid level of the evaporator at a constant from its base by adjusting the working fluid flow rate from the storage tank [3]. A shell-and-tube type heat exchanger was used for the superheater, considering the easiness of its connectivity to the evaporator. Compact brazed-type heat exchangers were used for the pre-heater and the condenser, considering the compactness of the system.

The gas-fired boiler used to produce steam, the heat source, was supplied by Hanshin Ltd. LNG was used as the fuel, producing a maximum output of 700 kW. The centrifugal pump, which comprises an impeller and is of the vertical type, was supplied by GRUNDFOS (model CR5-12A). The pump was connected with an inverter which adjusted its rotational speed by converting the frequency. The compact brazed heat exchangers were supplied by Janghan Engineers (model BC50-030 and GEA GmbH model WP10L-190 for the pre-heater and the condenser, respectively). The cooling tower was supplied by MEPS Ltd. The turbine was designed and manufactured in-house. The generator was supplied by Jinsol turbomachinary Ltd. [11]. The storage tank was designed in a cylindrical shape with a volume of 180 L, and was manufactured in-house.

2.2. Turbine design

The radial type turbine was designed as an expander considering the small flow rate of the working fluid, its high expansion ratio (4.11), and its small capacity. The characteristics of the working fluid in the turbine's design are as follows and are included in Table 3 below. It is susceptible to choking at the nozzle because its speed of sound is low, while the Re is high because its dynamic viscosity is low. The density of the working fluid is high, and the turbine size can be reduced.

Table 6
Design specifications of model turbine (working fluid is air).

Parameters	Unit	Value
Power capacity	kW	190
Rotational speed	rpm	63,000
Mass flow rate	kg/s	0.6
Total expansion ratio		3.6
Total isentropic efficiency	%	84
Nozzle inlet radius	mm	124
Nozzle vane height	mm	10
Nozzle-throat area	mm^2	1366
Rotor inlet radius	mm	90
Rotor exit radius at tip	mm	60
Rotor exit radius at hub	mm	22

The preliminary design of the turbine was conducted by considering the thermodynamic properties of the working fluid and the cycle operation condition in order to calculate its size, number of blades, angle of blades, etc. As the design requirements, the temperatures and pressures at the turbine inlet and outlet, output power, rotation speed and expected efficiency are shown in Table 4.

As the design results, the design parameters of the turbine blade and nozzle are shown in Table 5 [30]. A three-dimensional turbine blade was designed based on the geometrical similarity of the existing model turbine and the preliminary design results. Table 6 shows the design specifications of the model turbine, while Figs. 4 and 5 show a drawing and a photograph of the developed turbine blade and nozzle, respectively.

The turbo generator was developed by combining the turbine blade with the generator; it is composed of a turbine blade, a nozzle, a volute, a diffuser and a generator. The turbine blade was connected to the rotor of the generator directly without a speed reduction gearbox to reduce mechanical loss, as shown in Fig. 6(a). The blade was made of aluminum, which has the merits of ease of machining and light weight. A brushless synchronous-type generator employing a permanent magnet rotor was applied in consideration of its high rotational speed, i.e., 20,000 rpm under normal operating condition, and its compactness in terms of mechanical configuration, weight and size. Fig. 6(b)–(d) shows a drawing and a photograph of the developed turbo generator, respectively. The generated electricity was designed to be consumed by the load bank shown in Fig. 7(a).

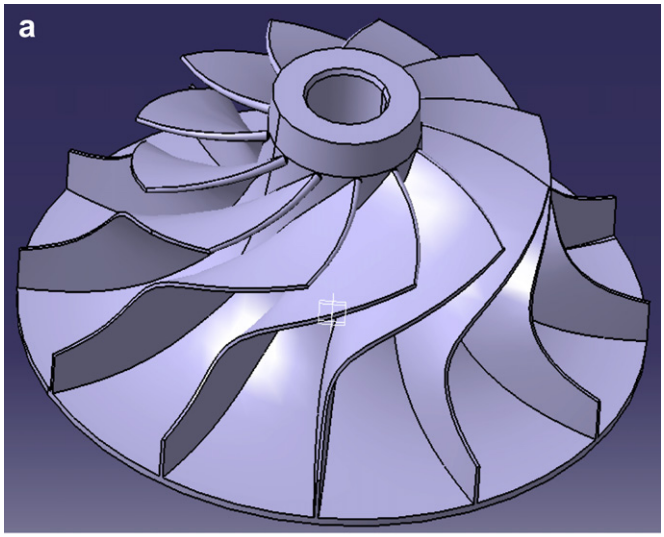

Drawing

Photograph

Fig. 4. Drawing and photograph of the turbine blade. (a) Drawing; (b) Photograph.

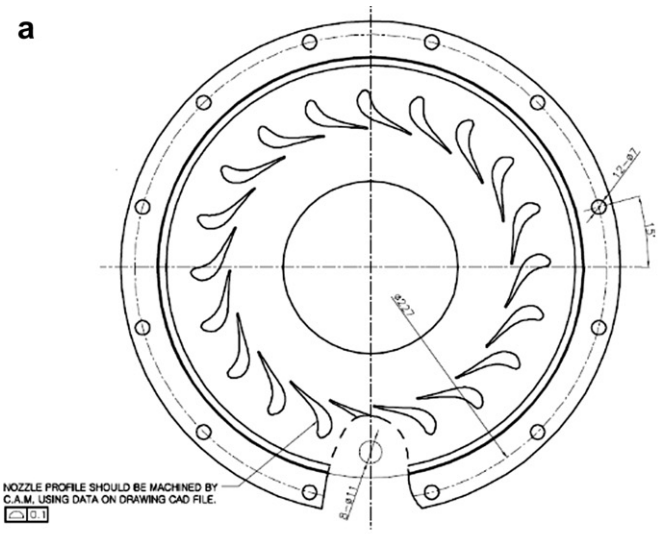

Drawing

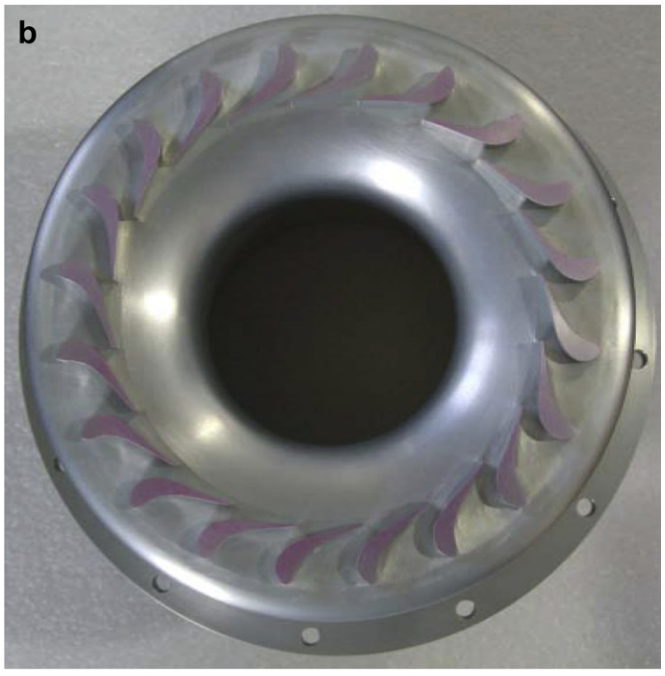

Photograph

Fig. 5. Drawing and photograph of the nozzle. (a) Drawing; (b) Photograph.

3. Experimental apparatus and method

Experiments were conducted to assess the performance of the designed ORC under a range of conditions. The experimental apparatus consists of the ORC system discussed in the previous

Rotor

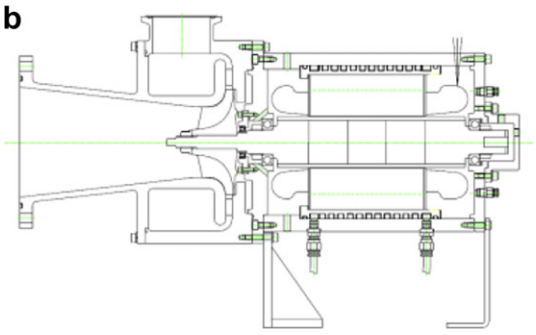

2-D drawing

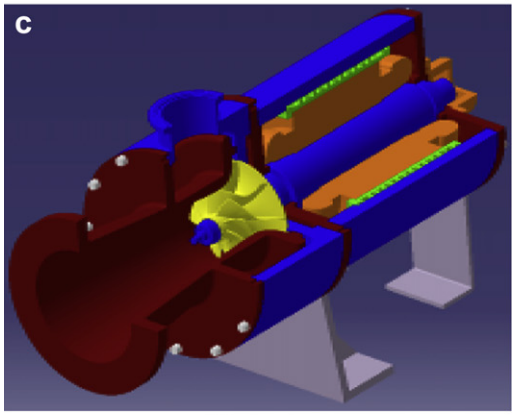

3-D drawing

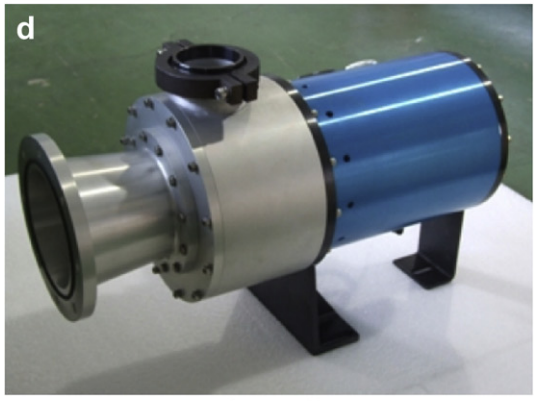

Photograph

Fig. 6. Drawing and photograph of turbo generator. (a) Rotor; (b) 2-D drawing; (c) 3-D drawing; (d) Photograph.

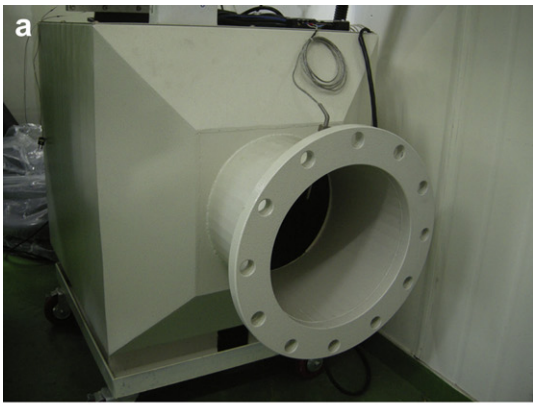

Load bank

Control panel

Fig. 7. Photographs of load bank and control panel. (a) Load bank; (b) Control panel.

section. The evaporator and superheater temperatures are controlled by valves installed in the three heat exchangers, and adjust the flow rate of the heat source, i.e., the steam produced by the boiler. The valves are controlled using PID logic on the basis of the working fluid temperature at the three heat exchanger outlets. The evaporation and condensation pressures of the cycle are saturation values, and are controlled by the temperatures of the working fluid in the evaporator and at the condenser outlet, respectively. The working fluid was to be circulated through the by-pass line instead of driving the turbine in the start-up stage before the whole system was heated up. Although a pre-heater was installed, it was not used as its control valve frequently repeated the opening and closing processes.

The experimental data were measured for 3 evaporation temperature steps, which were set at 77, 80 and 83 °C in the control panel shown in Fig. 7(b), to investigate the performance of the developed system near to its design condition with an average outdoor air temperature of 21 °C. A steady state was maintained for 15 min to gather data in each evaporation temperature step. The superheater outlet temperature was set 3 °C higher than the evaporation temperature in all the temperature steps.

During the operation, the thermodynamic properties of the working fluid in cycle were calculated by REFROPP 8.0 [24] using measured temperatures and pressures values. The sensors for measuring temperature, pressure, flow rate and electric power were installed in the cycle, as shown in Fig. 1. All temperatures were measured with a type T thermocouple with an accuracy of ±0.5 °C (made by SSK). All pressures were measured with pressure transducers made by Valcom (model VPRQ-A2-4C), with accuracy of ±0.25% over the full scale range (1.0 Mpa). The flow rate of the working fluid was measured using a turbine-type flow meter made by Blancett (model B111-110/B-2500) with an accuracy of ±0.5%. The electric power output of the generator was measured using a power analyzer made by Yokogawa (model WT3000), with accuracy of ±0.02%. All the measurement data were recorded and stored on a computer by using NI CompactDAQ, a data acquisition system.

This cycle operation condition was designed to determine the cycle layout and the specific design values of the main components, namely, the heat exchangers, turbine, pump, heat source and cooling system, etc. It is difficult to operate the cycle with this designed condition exactly, because there are several factors – such as atmospheric air temperature that cannot be controlled and which affect the cooling water temperature. And the condensation temperature could not be controlled as the cooling water flow rate was not controlled. The flow rate of the cooling water was maintained at its full capacity which was about 10 kg/s. Furthermore, the turbine efficiency affecting the cycle performance cannot be predicted exactly in the design procedure, or controlled artificially. It varies according to the pressure and temperature conditions of the turbine inlet and outlet, and influences the working fluid flow rate, electric power output, and cycle efficiency, etc.

4. Results and discussion

Table 7 shows the experimental results for the temperatures, pressures and thermodynamic properties, and the results are time average values in the key measurement positions when the average evaporator temperatures are 77.1, 79.5 and 82.3 °C, respectively. The measured evaporator temperatures show a small difference with the input values of the evaporator temperatures, which are 77, 80 and 83 °C. The thermodynamic properties – enthalpy, entropy and density – were calculated by REFPROP 8.0 [24] based on the measured temperatures and pressures, and their average values are given in Table 7.

The liquid state working fluids were supplied to the evaporator from the storage tank by a pump, then heated to vapor whose average temperatures and pressures were 77.1 °C and 7.60 bar, 79.5 °C and 8.04 bar, 82.3 °C and 8.64 bar, respectively, for the three evaporator temperature cases. Fig. 8(a) shows evaporator pressure versus evaporator temperatures, and the pressures increase to the temperatures.

The average turbine inlet (its position is same to that of the superheater outlet) temperatures were 80.7, 83.0, 85.4 °C, and they are about 3.6, 3.5 and 3.1 °C higher than the evaporator temperatures in the three cases, respectively. Though not shown in a figure, the pressures at the turbine inlet were almost the same as those at the evaporator, and their average values were the same as those in the evaporator, as shown in Table 7. The corresponding saturation pressures calculated by REFPROP 8.0 [24] were 8.03, 8.50 and 9.01 bar when the temperatures were the same as the turbine inlet temperatures, which were 80.7, 83.0 and 85.4 °C, respectively. The pressure values were 0.43, 0.46 and 0.36 bar higher than the measured values in the three evaporator temperature cases. Therefore, it is thought that the working fluids were changed into superheated vapor via the superheater in all three cases of evaporator temperature.

The working fluids at the turbine outlet were found to be superheated vapors as their pressures – 2.91, 3.03, and 3.17 bar – were lower than the corresponding saturation pressures, i.e., 4.76, 4.95, 5.11 bar, at the turbine outlet temperatures, which were 61.0, 62.4, 63.5 °C in the three evaporator temperature cases, respectively; and the degrees of superheat at the turbine outlet were greater than those at the turbine inlet in all three cases. The main

Tables 7
Experimental results of thermodynamic properties of working fluid.

Evaporator input temperature	Position	Temperature (°C)	Pressure (bar)	Enthalpy (kJ/kg)	Entropy (kJ/kg-K)	Density (kg/m^3)
77 °C	Evaporator	77.1	7.60	459	1.77	42.7
	Turbine inlet	80.7	7.60	463	1.79	41.8
	Turbine outlet	61.0	2.91	454	1.81	15.1
	Condenser outlet	37.4	2.34	249	1.17	1304
80 °C	Evaporator	79.5	8.04	461	1.78	45.2
	Turbine inlet	83.0	8.04	465	1.79	44.2
	Turbine outlet	62.4	3.04	455	1.81	15.8
	Condenser outlet	38.9	2.44	251	1.17	1300
83 °C	Evaporator	82.3	8.65	462.6	1.78	48.8
	Turbine inlet	85.4	8.65	466.3	1.79	47.8
	Turbine outlet	63.5	3.18	455.6	1.81	16.6
	Condenser outlet	40.3	2.54	252.9	1.18	1296

reason for this is that the working fluid expands when it passes through the turbine [3].

The working fluids at the condenser outlet were seen to change to an almost saturated liquid state, although their pressures, i.e., 2.34, 2.44 and 2.54 bar, were slightly higher than the corresponding saturation pressures, i.e., 2.30, 2.42 and 2.52 bar, at the condenser outlet temperatures, which were 37.4, 38.9 and 40.2 °C, respectively. Then the working fluids are supplied to the storage tank and to the evaporator through the pump. Though not shown in figure, the temperatures and pressures in the storage tank were almost the same as those at the condenser outlet, and their average values were the same as those at the condenser outlet in all the evaporator temperature cases.

Fig. 8(b) shows the turbine and condenser outlet pressures versus the evaporator temperature. Both of the pressures increased to evaporator temperatures. The pressures at the turbine outlet were greater than those at the condenser outlet, as shown in Fig. 8(b) and Table 7 in all cases. This is attributable to the pressure loss in the condenser. This irreversibility reduces the enthalpy drop in the turbine, as well as its power output and cycle efficiency.

Fig. 9 shows the pressure ratio between the turbine inlet and the outlet versus the evaporator temperature. The pressure ratio increased to the evaporator temperature, and the average values of the pressure ratio were 2.62, 2.65 and 2.72 when the average evaporator temperatures were 77.1, 79.5 and 82.3 °C, respectively. The three pressure ratios were lower than the design value of 4.11,

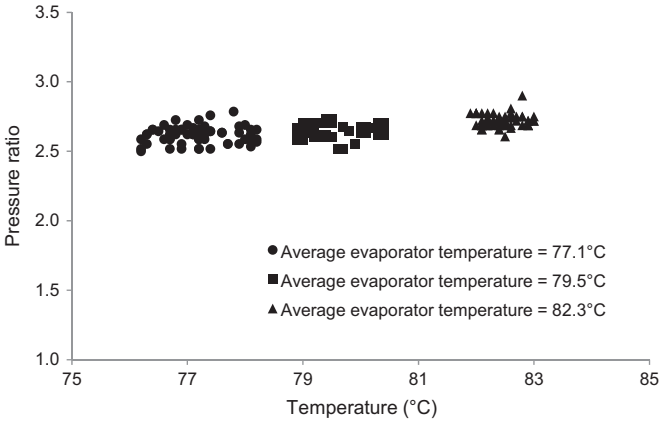

Fig. 9. Pressure ratio between turbine inlet and outlet versus evaporator temperature.

because the condensation pressures were higher than the design value.

Fig. 10 shows the mass flow rates versus the evaporator temperature. The mass flow rates increased to the evaporator temperatures, and their average values were 2.24, 2.37 and 2.56 kg/s when the average evaporator temperature was 77.1, 79.5 and 82.3 °C, respectively.

Fig. 11 shows the electric power outputs that were generated by the generator and measured by the power meter versus evaporator

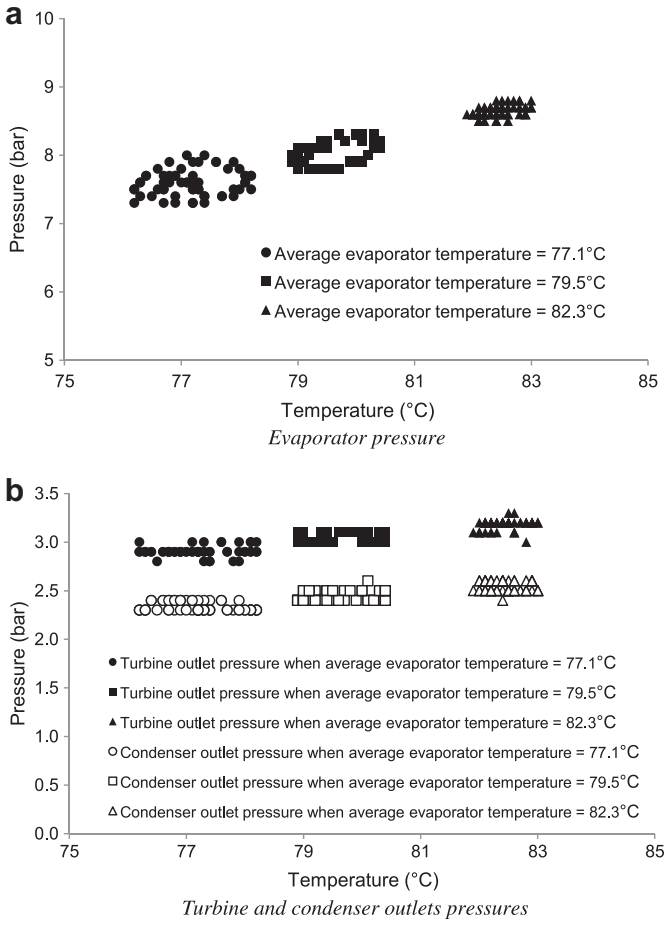

Fig. 8. Pressures versus evaporator temperature. (a) Evaporator pressure; (b) Turbine and condenser outlets pressures.

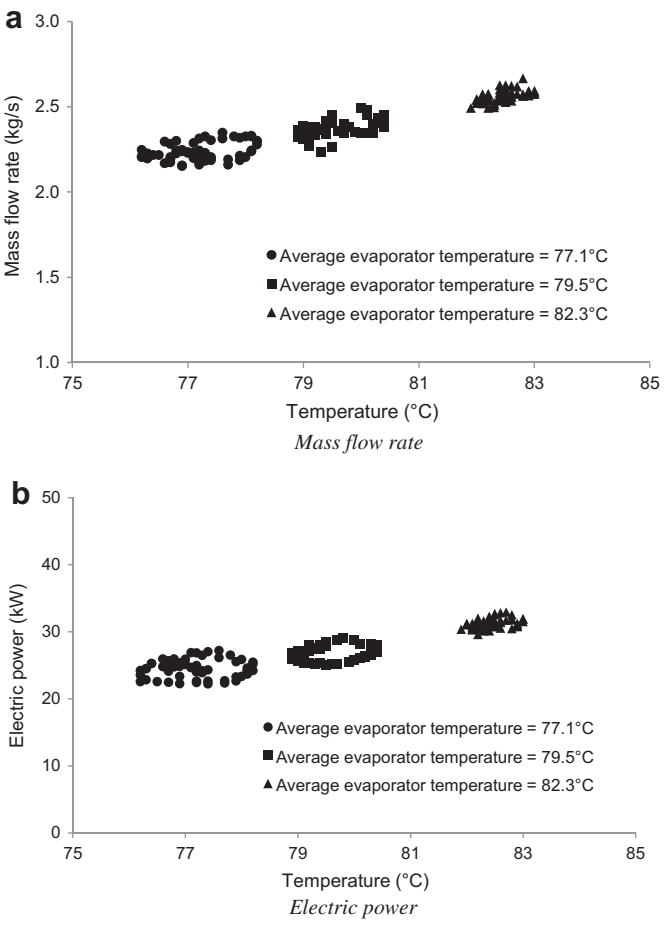

Fig. 10. Mass flow rate and electric power versus evaporator temperature. (a) Mass flow rate; (b) Electric power.

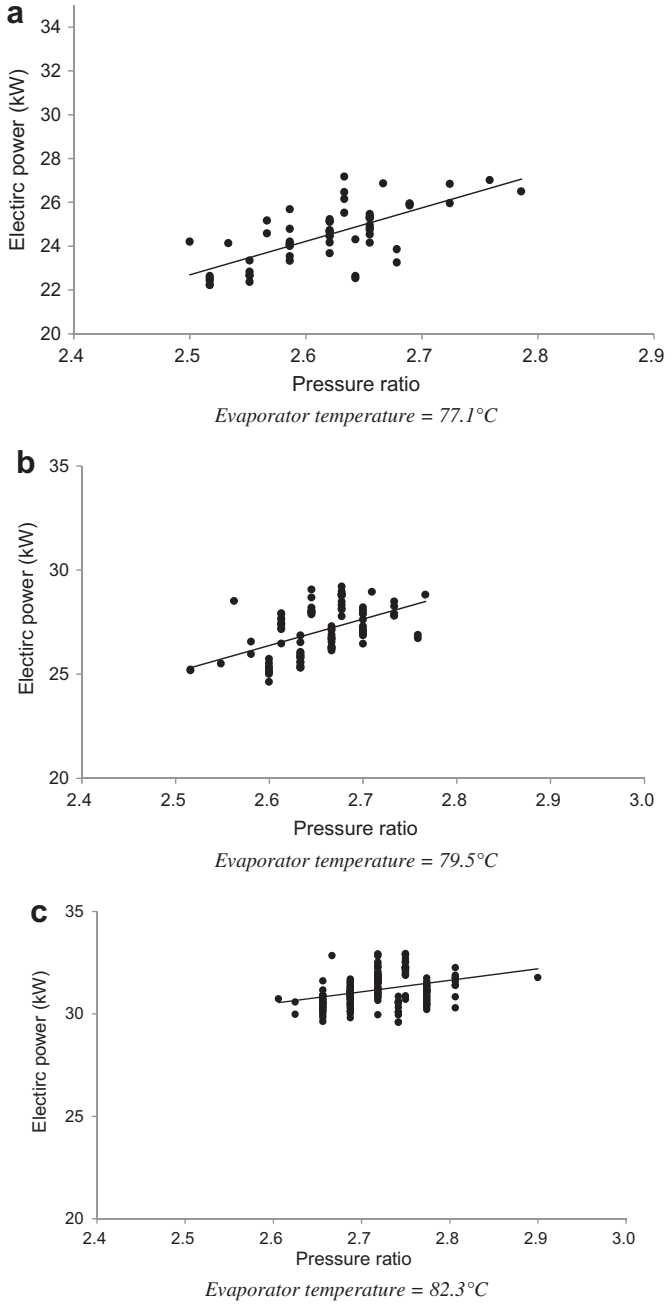

Fig. 11. Electric power output versus pressure ratio. (a) Evaporator temperature = 77.1 °C; (b) Evaporator temperature = 79.5 °C; (c) Evaporator temperature = 82.3 °C.

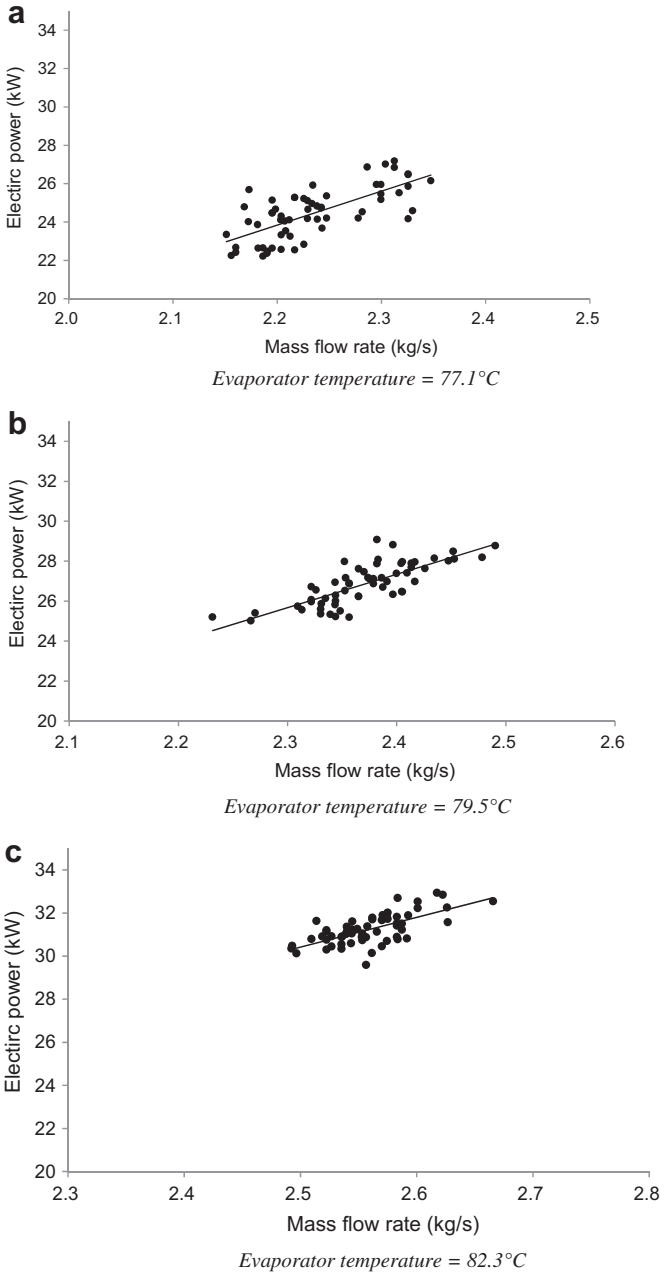

Fig. 12. Electric power output versus mass flow rate. (a) Evaporator temperature = 77.1 °C; (b) Evaporator temperature = 79.5 °C; (c) Evaporator temperature = 82.3 °C.

temperatures. The average electric power values were 24.5, 26.9 and 31.2 kW when the average evaporator temperature was 77.1, 79.5 and 82.3 °C, respectively. The electric power increased as the evaporator temperatures increased, because the pressure ratio between the turbine inlet and outlet, and the mass flow rate, increased to the evaporator temperature, as shown in Figs. 9 and 10(a), respectively.

Figs. 11 and 12 show the electric power versus pressure ratios between the turbine inlet and outlet, and the mass flow rate when the evaporator temperatures were 77.1, 79.5 and 82.3 °C, respectively. These figures show that the electric power increases to the pressure ratio between the turbine inlet and outlet, and the mass flow rate.

Fig. 13(a) shows the turbine and cycle efficiencies versus evaporator temperature, which were obtained using Equations (1) and (3), respectively [29].

$$\eta_t = \frac{\dot{W}_t}{\dot{m}\cdot(h_{t,i} - h_{t,o,is})} \tag{3}$$

where η_t is turbine efficiency, $h_{t,i}$ is the specific enthalpy of the working fluid at the turbine inlet, and $h_{t,o,is}$ is the specific enthalpy of the working fluid at the turbine outlet when its entropy is the same as that at the turbine inlet.

The average turbine efficiencies were 76.0, 77.5 and 82.2% and the average cycle efficiencies were 5.05, 5.24 and 5.66% when the average evaporator temperatures were 77.1, 79.5 and 82.3 °C, respectively.

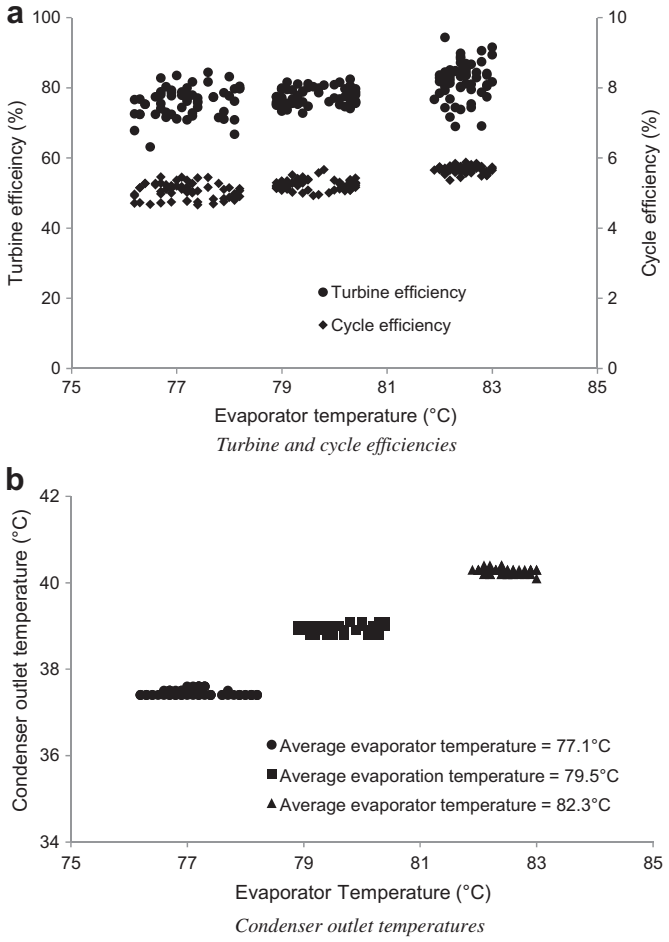

Fig. 13. Efficiencies and condenser outlet temperatures with evaporator temperature. (a) Turbine and cycle efficiencies; (b) Condenser outlet temperatures.

Cycle efficiency can be increased as the condensation temperature and the pressure are lowered by increasing the flow rate of cooling water. But in this study, the flow rate of the coolant was not controlled, but was maintained at its full capacity regardless of the cycle operation condition, as explained in Section 3 [31]. Therefore, the condenser outlet temperatures increased as the evaporator temperature increased, as in Fig. 13(b), which shows the condenser outlet temperatures versus evaporator temperature.

The maximum average electric power output of 31.2 kW, obtained at an average evaporator temperature of 82.3 °C, was almost consistent with the assumed value that is 30 kW in the cycle design procedure. This was compensated by the higher evaporator temperature and mass flow rate of the working fluid, although the cycle efficiency was lower than the design specification during the experiments [2].

The limitation of the cycle efficiency can be partly explained by the low temperature of the heat source. This could be improved by using heat sources with a higher temperature. In other words, an increase of the boiler-condenser saturation temperature difference would increase the Carnot efficiency of the cycle; and an increase of the boiler saturation temperature would raise the Carnot efficiency of the cycle [1]. A lower turbine outlet pressure leads to a greater enthalpy drop, thus increasing the ORC's efficiency [9]. The Carnot efficiency, η_C, for a heat engine operating between the temperatures of an evaporator and a condenser is calculated by applying the experimental results to Equation (4) [11,29].

$$\eta_C = \left(1 - \frac{\text{Condensation temperature(K)}}{\text{Evaporation temperature(K)}}\right) \times 100 \quad (4)$$

Although the average condensation and evaporator temperature values obtained in the experiment and written in Table 7 were not the exact saturation temperatures, they were substituted to Equation (4). The calculated Carnot efficiencies were 11.3, 11.5 and 11.8% when the average evaporator temperatures were 77.1, 79.5 and 82.3 °C, respectively.

The uncertainty in the measurement was computed by using the root-sum-square method [2,33]. The percent uncertainties of the turbine and the cycle efficiencies are lower than 2.24% and 2.34%, respectively.

5. Conclusion

In this study, an ORC that generates electric power and uses R245fa as the working fluid was designed and developed. A radial turbine coupled with a high-speed generator was designed by considering the thermodynamic properties of the working fluid and the cycle conditions. The performance of the developed cycle was investigated experimentally, and the factors which influence the performance of the developed ORC are analyzed and discussed. The maximum average cycle, turbine efficiencies, and electric power were found to be 5.22%, 78.7% and 32.7 kW, respectively.

The ORC developed in this study and the experimental results may serve as tools for the further optimization of ORCs. Further work will be conducted with a view to increasing overall cycle efficiency by increasing turbine efficiency, reducing heat and pressure losses in the flow path, and optimizing the system layout and components such as heat exchangers and a pump.

References

[1] Quoilin S, Lemort V, Lebrun J. Experimental study and modelling of an Organic Rankine Cycle using scroll expander. Applied Energy 2010;87:1260–8.
[2] Wang H, Peterson R, Harada K, Miller E, Ingram R, Fisher L, et al. Performance of a combined organic Rankine cycle and vapor compression cycle for heat activated cooling. Energy 2011;36(1):447–58.
[3] Yamamoto T, Furuhata T, Arai N, Mori K. Design and testing of the Organic Rankine Cycle. Energy 2001;26:239–51.
[4] Kang H. Organic Rankine cycle technology. Journal of the KSME 2009;49: 47–52.
[5] Dai Y, Wang J, Gao L. Parametric optimization and comparative study of organic Rankine cycle (ORC) for low grade waste heat recovery. Energy Conversion and Management 2009;50:576–82.
[6] Wei D, Lu X, Lu Z, Gu J. Performance analysis and optimization of organic Rankine cycle (ORC) for waste heat recovery. Energy Conversion and Management 2007;48:1113–9.
[7] Hung T, Shai T, Wang S. A review of organic Rankine cycles (ORCs) for the recovery of low-grade waste heat. Energy 1997;22:661–7.
[8] Quoilin S, Lemort V. Technological and economical survey of organic Rankine cycle systems. In: 5th European conference economics and management of energy in industry; 2009.
[9] Pei G, Li J, Li Y, Wang D, Ji J. Construction and dynamic test of a small-scale organic Rankine cycle. Energy 2011;36:3215–23.
[10] Bini R, Guercio A, Duvia A. Organic Rankine Cycle (ORC) in biomass applications for cogenerative systems in association with adsorption chillers. In: Proceedings of the 5th Dubrovnik conference on sustainable development of Energy. Croatia: Water and Environment Systems, Dubrovnik University; 2009.
[11] Nguyen V, Doherty P, Riffat S. Development of a prototype low-temperature Rankine cycle electricity generation system. Applied Thermal Engineering 2001;21:169–81.
[12] Manolakos D, Kosmadakis G, Kyritsis S, Papadakis G. On site experimental evaluation of a low-temperature solar organic Rankine cycle system for RO desalination. Solar Energy 2009;83:646–56.
[13] Larjola J. Electricity from industrial waste heat using high-speed organic Rankine cycle (ORC). International Journal of Production Economics 1995;41: 227–35.
[14] Maizza V, Maizza A. Unconventional working fluids in organic Rankine cycles for waste energy recovery systems. Applied Thermal Engineering 2001;21: 381–90.
[15] Brasz L, Bilbow W. Ranking of working fluids for organic Rankine cycle applications. In: Proc. of the Int. Refrigeration Eng. Conf. at Purdue; 2004.

[16] Brasz L. Assessment of C6F as working fluid for organic Rankine cycle applications. In: Proc. of the Int. Refrigeration Eng. Conf. at Purdue; 2008.
[17] Angelino G, Colonna P. Multicomponent working fluids for organic Rankine cycles (ORCs). Energy 1998;23:449–63.
[18] Hung T. Waste heat recovery of organic Rankine cycle using dry fluids. Energy Conversion and Management 2001;42:539–53.
[19] Liu B, Chien K, Wang C. Effect of working fluids on organic Rankine cycle for waste heat recovery. Energy 2004;29:1207–17.
[20] Hung T, Shai T, Wang S. A review of organic Rankine cycles (ORCs) for the recovery of low-grade waste heat. Energy 1997;22:661–7.
[21] Hung T, Wang S, Kuo C, Pei B, Tsai K. A study of organic working fluids on system efficiency of an ORC using low-grade energy sources. Energy 2010;35:1403–11.
[22] Hettiarachchi H, Golubovic M, Worek W, Ikegami Y. Optimum design criteria for an organic Rankine cycle using low-temperature geothermal heat sources. Energy 2007;32:1698–706.
[23] Isam H, Aljundi. Effect of dry hydrocarbons and critical point temperature on the efficiencies of organic Rankine cycle. Renewable Energy 2011;36(4):1196–202.
[24] Lemmon E, Huber M, McLinden M. NIST REFPROP standard reference database 23. Version 8.0. User's guide. NIST; 2007.
[25] Rayegan R, Tao Y. A procedure to select working fluids for Solar Organic Rankine Cycles (ORCs). Renewable Energy 2011;36(2):659–70.
[26] Suna J, Li W, Reddy A. Operation optimization of an Organic Rankine Cycle (ORC) heat recovery power plant. Applied Thermal Engineering 2011;31(11–12):2032–41.
[27] Bahaa S, Koglbauer G, Martin W, Johann F. Working fluids for low-temperature organic Rankine cycles. Energy 2007;32:1210–21.
[28] Huang T. Waste heat recovery of organic Rankine cycle using dry fluids. Energy Conversion and Management 2001;42(5):539–53.
[29] Wylen G, Sonntag R, Borgnakke C. Fundamentals of classical thermodynamics. 4th ed. New York: John Wiley & Sons, Inc.; 1993.
[30] Balje OE. Turbomachines – a guide to design, selection, and theory. New York: John Wiley & Sons, Inc.; 1981.
[31] Cho S, Cho C, Kim C. Performance characteristics of a turbo expander substituted for expansion valve on air-conditioner. Experimental Thermal and Fluid Science 2008;32:1655–65.
[32] Kane M, Larrain D, Favrat D, Allani Y. Small hybrid solar power system. Energy 2003;28:1427–43.
[33] Figliola R, Beasley D. Theory and design for mechanical measurements. 3rd ed. New York: John Wiley & Sons, Inc.; 1995.